FULL PAPER

Morphology Controlled Poly(aminophenylboronic acid) Nanostructures as Smart Substrates for Enhanced Capture and Release of Circulating Tumor Cells

*Jun Ouyang, Ming Chen, Wen-Jing Bao, Qian-Wen Zhang, Kang Wang, and Xing-Hua Xia**

A strategy is proposed to achieve an enhanced capture efficiency of and low damage to human leukemic lymphoblasts (CCRF-CEM) by the synergistic effect of topographical interactions and phenylboronic acid functional groups on nanostructures. To realize this purpose, a simple and template free method to synthesize boronic acid derivative polyaniline bioinspired nanostructures with controlled morphology is established. Different nanostructured morphologies such as nanotexture, nanofibers, nanoparticles, microsphere, and 3D porous network have been prepared by controlling the nucleation and growth rate for polymerization. The phenylboronic acid functional groups on the surface of the nanostructures during polymerization are used as artificial lectins to reversibly capture and release circulating tumor cells (CTCs) with little damage to the cells. The method presented here is simple, rapid, and highly efficient for CTC capture and release with low cost in materials and instruments.

1. Introduction

Cancer is one of the main causes of death for human beings and 90% of cancer-related deaths are caused by cancer metastasis.[1] Circulating tumor cells (CTCs) are the metastatic cancer cells shed from the primary tumor site and circulate in the peripheral blood to form secondary tumor in human body which finally lead to death.[2] Therefore, detection and isolation of CTCs in human blood is of great significance for cancer diagnosis and therapy in the early stage.

Traditional technologies for CTCs detection and isolation are based on the physical or chemical properties of the cells. The methods of filtration,[3] density gradient centrifugation,[4] flow cytometry,[5] or dielectrophoresis[6] are based on the size, density, charge, or migratory properties of cells. The immunomagnetic separation method[7] is based on the cell adhesion molecules expressed on surface of cancer cells. However, the selectivity or the capture efficiency of these methods does not yet meet the practical application. Therefore, it remains challenging to develop methods for efficient capturing CTCs because of the extremely low concentration in the blood of patients.

The surface of cells and their microenvironment have many nanostructured morphology, such as nanoscaled villi and pseudopod, nanofiber nets which form the extracellular matrix (ECM) of the cells, fractal-like nanostructures in vasculature or on the surface of cancer cells.[8,9] These nanostructures significantly influence the interactions between the cancer cells and their microenvironment.[8] In recent years, various bioinspired nanostructures have been constructed to mimic the cellular microenvironment topographical interactions to improve the capture efficiency of CTCs, such as nanovilli-like silicon-nanopillar array,[10] transparent quartz nanowire (QNW) arrays[11] and polystyrene nanotube arrays,[12] ECM-like TiO_2 nanofiber[13] and nanotextured polydimethylsiloxane (PDMS) substrates,[14] fractal-like gold nanostructured interfaces,[9] leukocyte-like particles,[15] platelet-like polyaniline/polystyrene microspheres.[16] Some other nanostructured interfaces such as nanoroughened glass surface,[17] functionalized graphene oxide nanosheets,[18] and carboxylic acid group functionalized poly(3,4-ethylenedioxy) thiophenes (PEDOT-COOH) nanodots[19] have also been developed for detection and isolation of CTCs. These nanostructures showed enhanced capture efficiency due to the improved topographical interactions with the cells. However, most of the fabrication process of these bioinspired nanostructures are time consuming and need expensive instruments. In addition to the nanostructures, surface chemistry of the nanostructured interfaces also influences their affinity to the cells. The synergistic effect of nanotopography and surface chemistry significantly improves the capture efficiency of CTCs.[19] Meanwhile, through the modification of the nanostructures, CTCs can be released from the bioinspired nanostructured interfaces after capture by external stimulus. It is very important for subsequent study of the cancer metastasis and cancer therapy.[20] To ensure the integrity of the cells after release, new methods for capture and release of cells have been proposed using

Dr. J. Ouyang, M. Chen, Dr. W.-J. Bao, Q.-W. Zhang, Prof. K. Wang, Prof. X.-H. Xia
State Key Laboratory of Analytical Chemistry for Life Science and Collaborative Innovation Center of Chemistry for Life Sciences
School of Chemistry and Chemical Engineering
Nanjing University
Nanjing 210093, P. R. China
E-mail: xhxia@nju.edu.cn

DOI: 10.1002/adfm.201502420

© 2015 WILEY-VCH Verlag GmbH & Co. KGaA, Weinheim

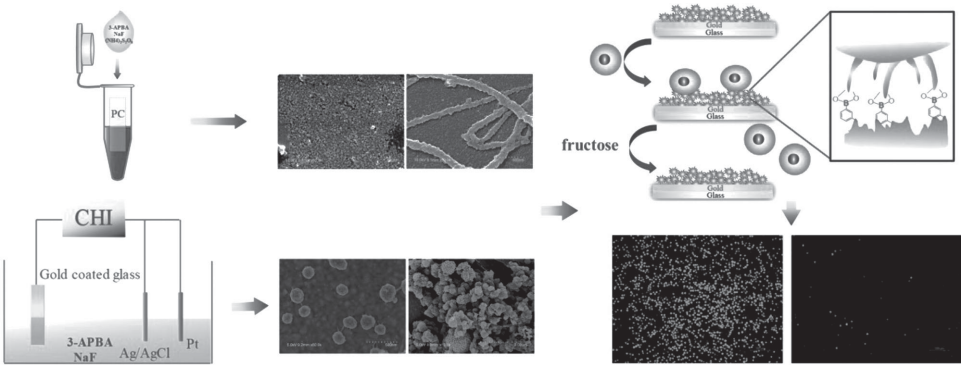

Figure 1. Illustration of the fabrication of different poly-APBA nanostructures and the process of capturing and releasing CTCs on the prepared nanostructures.

stimuli-responsive smart materials. The cell release process can be triggered by light,[21] heat,[22,23] electrochemistry,[24] magnetism,[25] solution pH,[26] nucleic acid,[20] fluid shear,[27] and degradable polymers.[28]

Among various substrates for cell release, boronic acid modified interfaces have attracted much attention due to the reversible covalent interactions of boronic acid. Boronic acid can reversibly react with 1,2- or 1,3-diols to form cyclic esters complexes.[29] It has been widely used in the detection of saccharides,[30–32] dopamine,[33] sialic acids,[34] and glycoprotein.[35,36] 3-Aminophenylboronic acid (3-APBA), an artificial lectins, which can reversibly bond to the glycan or sialic acid expressed on the extracellular membrane under mild conditions, is promising in cell isolation and analysis. It has been modified to nanostructured substrates for capture and release of CTCs with little damages to cells.[37–41] However, extra processes for fabrication of nanostructured substrates are needed for cell capture and the morphology of the nanostructures could not be well controlled yet.

Polymerization of 3-APBA monomer to acquire derivative polyaniline materials is a promising way to obtain boronic acid functional nanostructure interfaces in one step. Polyaniline (PANI) has been proved as one of the most promising polymer due to its ease of synthesis, low cost, wide range of conductivity, good biocompatibility, and better environmental stability.[42–44] Its controllable morphology, tunable physical and chemical properties make it fairly applicable in efficient and controllable CTCs capture and release. PANI can be polymerized through chemical or electrochemical methods and their morphology can be easily tuned by changing the ways of polymerization. Various shapes of PANI nanostructures have been synthesized using different conditions for polymerization.[45] However, only a few methods have been developed for the fabrication of poly(aminophenylboronic acid) (poly-APBA) nanostructures with controlled morphologies by polymerization of 3-APBA monomer. Deore et al. fabricated nanostructured poly-APBA with controlled morphology of nanoparticles and nanofibers using different solvent.[46,47] Li et al. fabricated U-shaped poly-APBA nanostructures using cetyltrimethylammonium bromide (CTAB) as the template.[48] However, there are few reports about the preparation of poly-APBA nanostructures with controlled morphologies on solid substrates without any templates.

Herein, we propose a simple and template-free method to synthesize boronic acid derivative PANI bioinspired nanostructures with controlled morphology by controlling the nucleation rate and growth process for polymerization of 3-APBA monomer. The fabrication of poly-APBA nanostructures and the process for capture and release of CTCs on the prepared nanostructures are presented in **Figure 1**. The morphology is easily tuned by changing the conditions for polymerization. Different nanostructured morphologies such as nanotexture, nanofibers, nanoparticles, microsphere, and 3D porous network can be prepared. The prepared poly-APBA nanostructures show enhanced capture and release efficiencies toward human leukemic lymphoblasts (CCRF-CEM) due to the synergistic effect of topographical interactions and phenylboronic acid functional group on the nanostructures. The phenylboronic acid functional groups on the surface of the nanostructures during polymerization are used as the artificial lectins to reversibly capture and release of CTCs with little damage to the cells. The method presented here is simple, rapid, and highly efficient for capture and release of CTCs with low cost in materials and instruments.

2. Results and Discussion

2.1. Fabrication and Characterization of Different Poly-APBA Nanostructures

The morphology of polyaniline is significantly affected by the nucleation and growth rates during polymerization of aniline. The rate for polymerization of substituted aniline is much slower compared to the polymerization of aniline because of the steric effects and the increasing electron withdrawing ability.[49] Polymerization of 3-APBA in the absence of F^- ions is very slow and there is almost no poly-APBA formed on the substrates in our experiments. It has been reported that F^- ions can catalyze the polymerization of 3-APBA by electronic or conformational perturbations caused by B–F^- interaction.[50] In order to obtain different morphologies of poly-APBA nanostructures, we change the concentration of F^- ions, the monomer concentration of 3-APBA and the electrochemical scanning rate to change the nucleation and growth rates for the polymerization of 3-APBA. Chemical polymerization method is simple and

© 2015 WILEY-VCH Verlag GmbH & Co. KGaA, Weinheim

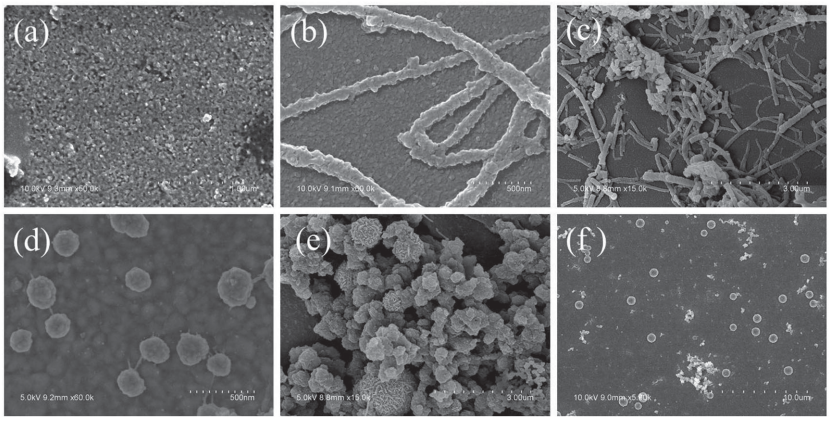

Figure 2. SEM images of the poly-APBA nanostructures prepared by a–c) chemical method and d–f) electrochemical method under different conditions. a) 40×10^{-3} M 3-APBA, 40×10^{-3} M NaF, 0.1 M $HClO_4$, and 20×10^{-3} M APS (CP-40APBA-40NaF); b) 100×10^{-3} M 3-APBA, 40×10^{-3} M NaF, 0.1 M $HClO_4$, and 20×10^{-3} M APS (CP-100APBA-40NaF); c) 100×10^{-3} M 3-APBA, 100×10^{-3} M NaF, 0.1 M $HClO_4$, and 20×10^{-3} M APS (CP-100APBA-100NaF); d) 20×10^{-3} M 3-APBA, 40×10^{-3} M NaF, and 0.5 M HCl at 20 mV s^{-1} (EP-20APBA-40NaF-20 mV); e) 20×10^{-3} M 3-APBA, 200×10^{-3} M NaF, and 0.5 M HCl at 20 mV s^{-1} (EP-20APBA-200NaF-20 mV); f) 20×10^{-3} M 3-APBA, 40×10^{-3} M NaF, and 0.5 M HCl at 100 mV s^{-1} (EP-20APBA-40NaF-100 mV).

in favor of large-scale synthesis. Thus, we first prepared poly-APBA nanostructures by chemical method. The morphology of the prepared poly-APBA nanostructures under different conditions was characterized by SEM. The influence of the monomer concentration of 3-APBA on the formation of poly-APBA nanostructures is shown in **Figure 2**a,b. When 40×10^{-3} M 3-APBA and 40×10^{-3} M NaF are used, the polymerization rate of poly-APBA is relatively slow. The formed structure (named as CP-40APBA-40NaF) under the conditions shows a nanotextured structure composed of cross-linked nanofiber/granule network (Figure 2a). However, when the concentration of 3-APBA is increased to 100×10^{-3} M, the polymerization rate increases significantly and visible polymerization in the solution can be seen in a few minutes. The poly-APBA nanostructure accordingly changes to loose cross-linked nanofiber network with nanofiber width of 90–150 nm (Figure 2b). The slow reaction rate of substituted aniline leads to formation of agglomerated granule or spheres because of the steric effects and the increasing electron withdrawing ability of substituted aniline while accelerating the reaction tends to formation of nanofibers.[51] The formation of different morphologies of poly-APBA nanostructures is due to the different nucleation and growth rates caused by different concentration of 3-APBA. When the concentration of 3-APBA is low, the nucleation and growth rates are slow, tending to the formation of compacted structure of nanofiber/granule network. The formation of nanofibers at increased concentration of 3-APBA is a result of the fast formation of reactive nuclei and the anisotropic growth of the reactive nuclei.[51]

Since F^- ions can catalyze the polymerization of 3-APBA, change of the F^- ions concentration will change the nucleation and growth rates during polymerization. As shown in Figure 2b,c, when the concentration of NaF is increased to 100×10^{-3} M, the nucleation and growth rates of 3-APBA become much faster than the polymerization rate of 3-APBA at 40×10^{-3} M NaF. Thus, the visible polymerization appears in a minute. The poly-APBA nanofibers grow disordered, forming many aggregates during the polymerization. The newly generated reactive intermediates are too much for anisotropic growth on existed nuclei and stack to each other forming aggregates.

Polymerization of 3-APBA by chemical polymerization method without templates tends to form flat membranes on solid substrates in our experiments. In the case of electrochemical method, the polymerization starts at the electrode surface and the film can be formed directly on the solid substrate, favoring the formation of three-dimensional structure. Therefore, we prepared poly-APBA nanostructures by electrochemical polymerization to obtain three-dimensional structures for cell capture and release. In electrochemical method, F^- ions can also change the nucleation and growth rates in the polymerization of 3-APBA, influencing the morphology of poly-APBA. As shown in Figure 2d,e, when the concentration of NaF is 40×10^{-3} M, the polymerization of 3-APBA on the working electrode (gold film coated glass slide) is very slow. The formed EP-20APBA-40NaF-20 mV shows a nanostructure consisted of dispersed nanoparticles with diameter around 200 nm (Figure 2d). When the concentration of NaF is increased to 200×10^{-3} M, the polymerization becomes much faster and a 3D porous network is formed. Slow potential scan rate and polymerization rate make the coupling of active intermediate species slowly and isotropically, which leads to the formation of nanoparticles.[52] The formation of dispersed nanoparticles at 40×10^{-3} M NaF may be due to the slow nucleation and growth rates together with the steric effects of substituted aniline. It takes more time for the generated active intermediate species to couple and rearrange to the most favorable form at low concentration of F^- ions. The polymerization rate of 3-APBA increases with the increasing concentration of F^- ions, thus, a 3D porous network is formed at 200×10^{-3} M NaF because of the accelerated polymerization rate of 3-APBA. Different to the chemical polymerization of 3-APBA, almost all of the new active intermediate species generated by electrochemical method are on the surface of the working electrode. The polymerization takes place at the nucleation center near the surface of the working electrode and the nanoparticles become larger to form a 3D porous network due to the growth of poly-APBA. The potential scan rate can change the number of nucleation center in the polymerization of 3-APBA and influence the morphology of the poly-APBA nanostructures. As shown in Figure 2d,f, when the potential scan rate is increased to 100 mV s^{-1}, the polymerization rate of 3-APBA is still relatively low due to the low concentration of F^- ions. However, the number of active intermediate species formed during electrochemical polymerization within each potential cycle is less and few reactive nuclei can be formed compared to the polymerization of 3-APBA at 20 mV s^{-1}. The subsequently generated active intermediate reacts with the existed nucleation center for continuous growing of poly-PABA nanostructures, resulting in the formation of microspheres with diam-

© 2015 WILEY-VCH Verlag GmbH & Co. KGaA, Weinheim

eter around 500 nm (Figure 2f). However, the density of microspheres is low, which is not capable for cells capture. Therefore, we choose compacted nanotexured membrane (CP-40APBA-40NaF), loose cross-linked nanofiber network (CP-100APBA-40NaF), dispersed nanoparticles (EP-20APBA-40NaF-20 mV), and 3D porous network (EP-20APBA-200NaF-20 mV) as the nanostructured substrates for capture of CTCs.

Raman spectroscopy was used to analyze the structure of different poly-APBA nanostructures. As shown in Figure S1 (Supporting Information), all of the poly-APBA nanostructures prepared here show the characteristic peaks of polyaniline.[53,54] The bands at 1174, 1597, 1640 cm^{-1} are assigned to the rings C–H bending modes, rings C–C stretching modes and rings C–C stretching modes, respectively. The bands appeared at 1334 and 1398 cm^{-1} indicate the presence of C–N•$^{+}$ polaron in the poly-APBA nanostructures. The peak at 1469 cm^{-1} is related to the stretching vibration of the C–N group. These results demonstrate that we successfully fabricated poly-APBA nanostructured films.

2.2. Capture of CTCs on Different Poly-APBA Nanostructured Substrates

Nanostructures on the surface of cells and the morphology of substrate can significantly influence the cell-substrate interactions. Thus, enhanced local topographic interactions between cells and substrate can significantly improve the capture efficiency.[8–10] Therefore, we fabricated poly-APBA nanostructures with different morphologies to enhance the interactions between cells and the nanostructured interfaces by topographical interactions to achieve a high capture efficiency. CCRF-CEM were captured on different poly-APBA nanostructured substrates, stained by AO and observed under a fluorescence inversion microscope. As shown in **Figure 3**a, there are few CCRF-CEM captured on a BSA blocked bare gold film coated glass slide, indicating a low CCRF-CEM capture efficiency on unmodified substrate. However, CCRF-CEM captured on a poly-APBA nanostructured substrate is much more than the bare gold film coated glass slide. The capture yields on EP-20APBA-40NaF-20 mV, CP-40APBA-40NaF, CP-100APBA-40NaF, EP-20APBA-200NaF-20 mV are 19.2%, 52.8%, 29.6%, 78.3%, respectively. The capture yields on EP-20APBA-40NaF-20 mV and CP-100APBA-40NaF are lower than the other two poly-APBA nanostructured substrates. It may be due to the relatively low density of nanoparticles and nanofibers formed on the gold film with less phenylboronic acid functional group on the poly-APBA nanostructured interfaces for cell capture. Compared to the flat nanotexured membrane (CP-40APBA-40NaF), a higher capture efficiency can be achieved on a 3D porous network (EP-20APBA-200NaF-20 mV), which is possibly due to the much more matched topographical interactions between the nanostructured interfaces and cells. Compared to glycan on cell surface, fructose can form a much more stable covalent bond to phenylboronic acid at pH 8.0. Addition of fructose will block the affinity of phenylboronic acid functional groups on the nanostructured interfaces for cells.[37,55] As shown in Figure 3f, the CCRF-CEM captured on EP-20APBA-200NaF-20 mV are significantly reduced when we block the phenylboronic acid functional groups on the poly-APBA nanostructured interfaces with fructose. These results demonstrate that the highest capture efficiency observed on EP-20APBA-200NaF-20 mV is a result of the synergistic effect of topographical interactions and phenylboronic acid functional group on the nanostructures.

2.3. SEM Characterization of the Captured CTCs on Different Poly-APBA Nanostructured Substrates

Pseudopod which contains cross-linked cytoskeletal actin bundles is known to be a critical organelle in the contact-guidance response of cell-substrate contact.[56] Cytoskeletal actin drives the pseudopods to propagate and elongate in response to the local topographic interactions between the nanostructured substrate and the cellular surface components.[57] When the local topographic interactions match well, more pseudopods can be produced to achieve a stable adhesion to the nanostructured substrate, indicating an enhanced interaction and an improved capture efficiency of cells.[10,56–58] To observe the morphology of

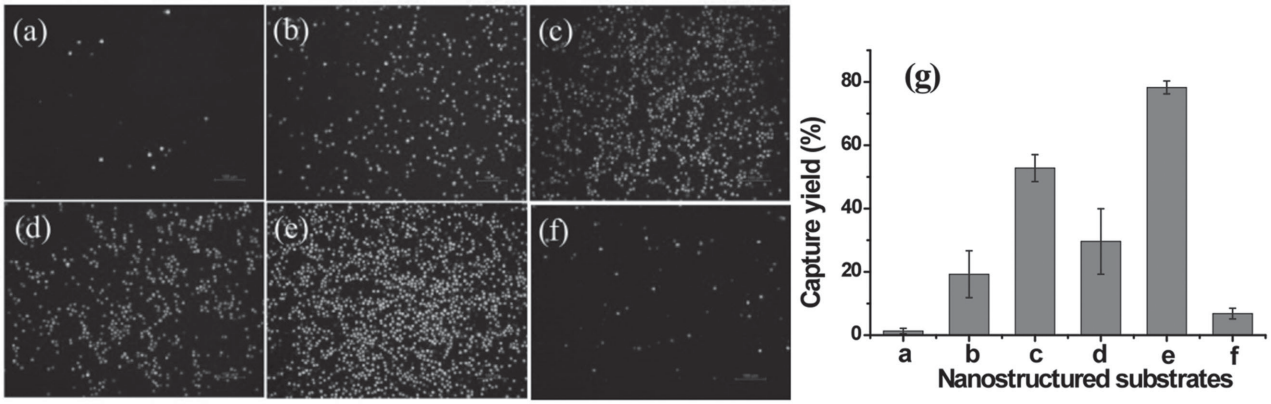

Figure 3. Fluorescent images of the captured CCRF-CEM on different poly-APBA nanostructured substrates. a) Bare gold film coated glass slide; b) EP-20APBA-40NaF-20 mV; c) CP-40APBA-40NaF; d) CP-100APBA-40NaF; e) EP-20APBA-200NaF-20 mV; f) Fructose blocked EP-20APBA-200NaF-20 mV. g) Capture yields of CCRF-CEM on different poly-APBA nanostructured interfaces.

© 2015 WILEY-VCH Verlag GmbH & Co. KGaA, Weinheim

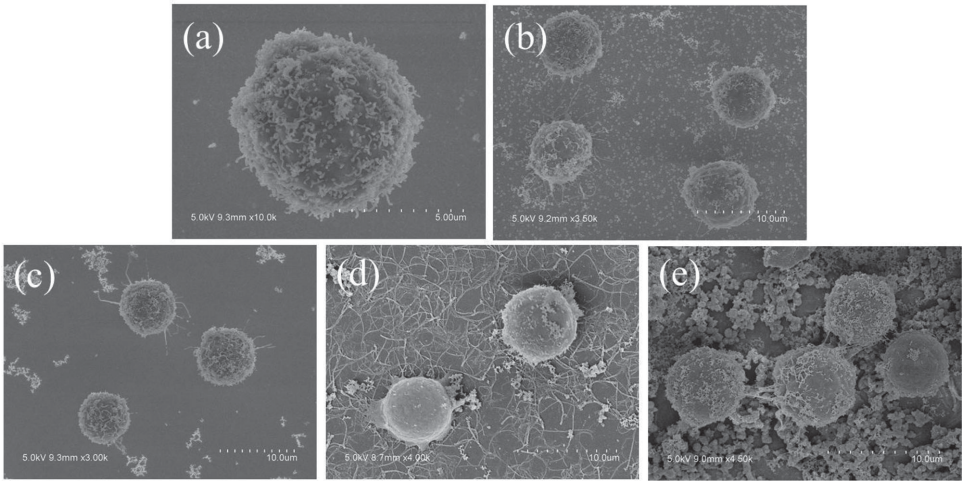

Figure 4. SEM images of the captured CCRF-CEM on different poly-APBA nanostructured substrates. a) Bare gold film coated glass slide; b) dispersed nanoparticles (EP-20APBA-40NaF-20 mV); c) compacted nanotextured membrane (CP-40APBA-40NaF); d) loose cross-linked nanofiber network (CP-100APBA-40NaF); e) 3D porous network (EP-20APBA-200NaF-20 mV).

CCRF-CEM captured on different poly-APBA nanostructured substrates and study the interactions between CCRF-CEM and the nanostructured interfaces, we used SEM to characterize the CCRF-CEM captured on different poly-APBA nanostructured interfaces. As shown in **Figure 4**a, there is nearly no pseudopod formed on the bare gold film, indicating a weak interaction between CCRF-CEM and gold film. The capture efficiency is low. However, when the poly-APBA nanostructures are used, much more pseudopods appear on the interfaces of the poly-APBA nanostructures, indicating an enhanced interaction between CCRF-CEM and poly-APBA interfaces due to the synergistic effect of phenylboronic acid on the interfaces and the topographical interactions (Figure 4b–e). EP-20APBA-200NaF-20 mV has the most amount of pseudopods (Figure 4e) because of its large specific surface area which provide more phenylboronic acid functional group for cell conjunction, much more matched topographical interactions and 3D space for pseudopods to spread. The results are in good agreement with the results obtained from fluorescence imaging. Thus, we choose the EP-20APBA-200NaF-20mV as the nanostructured substrate for capture and release of CTCs.

2.4. Conditions for CCRF-CEM Capture

Boronic acid can reversibly react with cis-diols to form cyclic esters complexes. It usually needs an alkaline condition to form a stable covalent bond.[37] To study the influence of pH on the cell capture, EP-20APBA-200NaF-20 mV was used as the substrate for CCRF-CEM capture at different pH values. The fluorescence images of CCRF-CEM captured on EP-20APBA-200NaF-20 mV at different pH values are shown in Figure S2 (Supporting Information). The number of cells captured on the EP-20APBA-200NaF-20 mV substrate increases with the increase of solution pH, indicating a much stronger and stable covalent bond formed at high pH values (**Figure 5**a). The number of cells captured on the nanostructured substrate increases quickly in the solution pH ranging from 7.4 to 8.0 due to the increased affinity of boronic acid to cells. With the further increase of pH, saturation of captured cells on the nanostructured substrate occurs, forming a monolayer of cells.[37,55] However, high pH will more or less cause damages to cells. Therefore, we choose pH 8.0 as the condition for cell capture.

To study the influence of time on the capture of CCRF-CEM, we incubated CCRF-CEM on the EP-20APBA-200NaF-20 mV substrate at different times from 5 to 60 min. The fluorescence images of CCRF-CEM captured on the EP-20APBA-200NaF-20 mV at different times are shown in Figure S3 (Supporting Information). The capture yield increases very quickly in the first 30 min and then slows down. The capture yield reaches 78.3% in 60 min (Figure 5b). Considering the capture of CCRF-CEM is performed under alkaline conditions, the capture time should not be too long. Thus, we choose 60 min as the capture time for capture of CCRF-CEM.

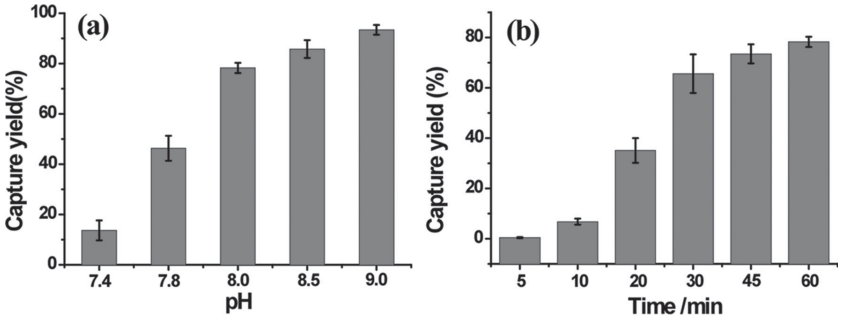

Figure 5. Capture yields of CCRF-CEM at a) different pH values and b) different capture times.

© 2015 WILEY-VCH Verlag GmbH & Co. KGaA, Weinheim

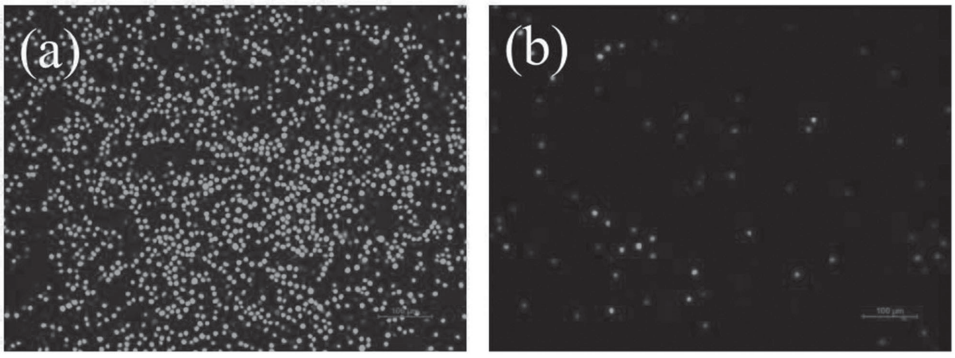

Figure 6. a) Capture and b) release of CCRF-CEM on the EP-20APBA-200NaF-20 mV nanostructured substrate.

2.5. Cell Release and Viability Analysis

Release of CTCs from the substrates after capture is important for subsequent study of the metastasis, mutation of CTCs and therapy of cancers. The releasing process should have little damages to CTCs. Here, we used fructose to release captured CCRF-CEM from the poly-APBA nanostructured interfaces. Fructose can form a stable covalent bond to boric acid and break the boric acid ester bond formed between CCRF-CEM and poly-APBA nanostructured interface to release the captured cells.[37,38] The fluorescent image in **Figure 6**a shows that CCRF-CEM are well captured on the poly-APBA nanostructured substrate. When fructose is added, most of the captured cells are released from the substrate with a release efficiency of 94.1% (Figure 6b). It demonstrates that the prepared poly-APBA nanostructured substrate is capable for efficient capture and release of CCRF-CEM.

Cell viability was studied by acridine orange (AO)/propidium iodide (PI) double staining analysis. AO can penetrate through the intact cell membrane and bond to DNA to show a strong green fluorescence. PI can only penetrate through the damaged cell membrane then bonds to DNA to show a red fluorescence. Thus, PI can be used as an indicator for dead cells. By AO/PI double staining, we can distinguish living cells from dead cells through different fluorescence. Cell viability of CCRF-CEM captured on the poly-APBA nanostructured substrate before release is shown in **Figure 7**a. We can see that most of the cells are alive before release. CCRF-CEM released from the substrates was collected, stained by AO/PI, dropped on the hemocytometer and observed by a fluorescence inversion microscope system. The cell viability remains more than 90% after release, as shown in Figure 7b. The cell viability changes little before and after release.

3. Conclusions

In summary, we propose a strategy to achieve an enhanced capture efficiency of CCRF-CEM by the synergistic effect of topographical interactions and phenylboronic acid functional groups on the nanostructures. Boronic acid derivative PANI bioinspired nanostructured interfaces with controlled morphology such as nanotexture, nanoparticles, microsphere, nanofiber, and 3D porous network have been prepared by controlling the nucleation and growth rates for polymerization. Phenylboronic acid functional groups on the surface of poly-APBA nanostructures during polymerization can be used for reversibly capturing and releasing CCRF-CEM under a mild condition. The prepared poly-APBA nanostructures show enhanced capture and release efficiencies toward CCRF-CEM with little damages to the cells. It is conceivable that the one-step method presented here provides a simple, rapid, and low cost approach to the fabrication of boronic acid functional nanostructures and the morphology could be further tuned by changing conditions for polymerization to mimic various cellular microenvironment topographical interactions. This method shows potential for s

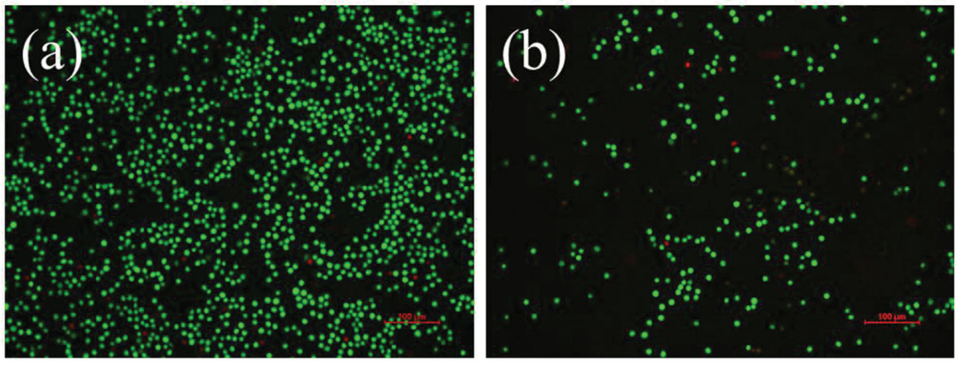

Figure 7. a) Cell viability analysis of CCRF-CEM captured on the poly-APBA nanostructured substrate before release. b) Cell viability analysis of CCRF-CEM on a hemocytometer after release.

© 2015 WILEY-VCH Verlag GmbH & Co. KGaA, Weinheim

highly efficient separation of CTCs, early diagnosis, and monitor of cancers, subsequent study of the metastasis, mutation, and therapy of cancers.

4. Experimental Section

Reagent and Instruments: Hydrochloric acid, sulfuric acid, perchloric acid, hydrogen peroxide, ammonium persulfate, and sodium fluoride were purchased from Nanjing Chemical Reagent Co. Ltd. (China). 3-Aminophenylboronic acid (3-APBA) and fructose were purchased from TCI Development Co. Ltd (Shanghai, China). Gold film coated glass slide purchased from Haoyue Quartz Co. (Lianyungang, China) was used as the working electrode for polymerization of 3-APBA. Polycarbonate was obtained from Suzhou Plastic Co. (China). Acridine orange (AO), propidium iodide (PI) and RPMI-1640 culture medium were obtained from KeyGEN BioTECH development Co. Ltd. Fetal bovine serum (FBS) and penicillin-streptomycin were purchased from Corning Inc. The CCRF-CEM (CCL-119, T cell line, human ALL) cell line was obtained from Shanghai Institutes for Biological Sciences (China). All aqueous solutions were prepared using deionized water (18 MΩ cm, Elix 5 Pure Water System, USA) and filtered through a 0.22 μm syringe filter prior to use. The morphology of prepared poly-APBA nanostructures and the cells captured on poly-APBA nanostructures were characterized using a scanning electron microscope (SEM, S-4800, Japan). Raman spectrometer (inVia-Reflex, UK) with an excitation wavelength of 633 nm was used to characterize the structures of poly-APBA. Electrochemical polymerization was performed on an electrochemical station (CHI 650a, China). Fluorescence imaging was taken by a fluorescence inversion microscope system (Leica, Dmire2, Germany).

Fabrication and Characterization of Poly-APBA Nanostructures with Different Morphologies: Different methods were used to fabricate poly-APBA nanostructures with controlled morphology by controlling the nucleation rate and growth process during polymerization. For electrochemical method, 20×10^{-3} M APBA monomer prepared in 0.5 M HCl was used for polymerization. Traditional three-electrode system was used to fabricate poly-APBA modified electrode using a gold film coated glass slide as the working electrode. A saturated Ag/AgCl and a platinum wire were used as the reference and counter electrodes, respectively. Before electrochemical polymerization, the gold film coated glass slide was sonicated in ethanol and deionized water for 5 min, respectively. Then, it was cleaned with H_2SO_4/H_2O_2 solution (volume ratio 3:1) at 100 °C for 1 h. The cleaned gold film slide was rinsed with deionized water and dried prior to use. Cyclic voltammetry was taken for electrochemical polymerization of 3-APBA within a potential window ranging from –0.1–1.1 V. Different concentrations of NaF (40×10^{-3} M, 200×10^{-3} M) and different potential scan rate (20 mV, 100 mV) were used to control the morphology of poly-APBA nanostructures. Electrochemical polymerization of 3-APBA experiences multiple steps. 3-APBA monomer was oxidized to a radical cation under an appropriate potential. Then, coupling and re-aromatization of the radical cation take place to form a dimer. The dimer is subsequently oxidized on the electrode surface. The generated dimer radical cation coupling with the monomer radical cation results in the chain propagation.[59,60] The prepared poly-APBA nanostructures were named as EP-20APBA-40NaF-20 mV, EP-20APBA-200NaF-20 mV, and EP-20APBA-40NaF-100 mV, respectively. For preparing poly-APBA nanostructures using chemical method, polycarbonate was used as the substrate for chemical polymerization. The polymerization was taken in 0.1 M $HClO_4$ solution at 4 °C for 3 h using ammonium persulfate (20×10^{-3} M) as the oxidant. Different concentrations of APBA (40×10^{-3} M, 100×10^{-3} M) and NaF (40×10^{-3} M, 100×10^{-3} M) were used to control the morphology of poly-APBA nanostructures. The prepared poly-APBA nanostructures were named as CP-40APBA-40NaF, CP-100APBA-40NaF, and CP-100APBA-100NaF, respectively. The poly-APBA nanostructures modified polycarbonate was rinsed with HCl (0.1 M), deionized water and dried prior to use. The fabricated poly-APBA nanostructured substrates were characterized by SEM and Raman spectrometer. Polymerization of 3-phenylboronic acid will take place on any surface contacting with the reaction mixture. To make sure that all of the areas of poly-APBA formed on every substrate are the same, we blocked the redundant surface of the substrates using polydimethylsiloxane (PDMS), leaving an area of 0.5×0.5 cm^2 containing poly-APBA nanostructures for cell capture.

Cell Culture: CCRF-CEM was cultured in RPMI-1640 medium containing glucose (2 g L^{-1}), L-Glutamine (0.3 g L^{-1}), sodium bicarbonate (2 g L^{-1}), penicillin (80 U mL^{-1}), streptomycin (0.08 mg mL^{-1}), and 10% serum at 37 °C under 5% CO_2.

Capture of CCRF-CEM on Different Poly-APBA Nanostructured Interfaces and Fluorescence Imaging: CCRF-CEM was centrifuged at 1000 rpm for 5 min and re-dispersed in PBS solution (pH 8.0). The concentration of CCRF-CEM was calculated using a hemocytometer and a final concentration of 3×10^6 cells mL^{-1} was obtained for cell capture experiments. The poly-APBA nanostructured substrates were incubated with 1% BSA solution to reduce nonspecific adsorption of cells. Capture of CCRF-CEM was performed by dropping 20 μL of CCRF-CEM solution onto different poly-APBA nanostructured substrates (0.5×0.5 cm). The cells were incubated at 37 °C for 60 min. Then, the substrates were rinsed with PBS for three times to remove unconjugated cells. The captured cells were stained by AO for 10 min, then washed using PBS and observed using a fluorescence inversion microscope system. Calculation of the capture yield of CCRF-CEM through fluorescence imaging is realized by counting the number of cells captured on poly-APBA nanostructures by ImageJ (National Institutes of Health, NIH) which is a software for processing images. The cells in the fluorescent images are selectively chosen via the image processing function of the software, and thus the number of cells can be counted using the analysis function of the software. According to the number of cells in the fluorescent images and the area of the fluorescent images, we can obtain the number of cells captured on the whole poly-APBA nanostructure, which is presented as $N_{capture}$. The total number of CCRF-CEM added to the poly-APBA nanostructure is calculated by the concentration and volume of CCRF-CEM, and is presented as N_{total}. The capture yield is defined as the ratio of $N_{capture}/N_{total}$.

SEM Characterization of Captured Cells on Different Poly-APBA Nanostructured Interfaces: To observe the detailed morphology of cells captured on different poly-APBA nanostructured interfaces, SEM images were taken to characterize the morphology of captured cells in detail. The preparation process of the samples for electron microscopy observation is described as follows: First, the captured cells were immobilized tightly onto the different poly-APBA nanostructured substrates using 2.5% glutaraldehyde for 5 h. Then, the captured cells were gradiently dehydrated using ethanol with different concentrations (30%, 50%, 70%, 90%) for 10 min each. After that, 0.5% uranyl acetate was used to stain the cells for 0.5 h to enhance the contrast for SEM observation. Then, the cells were further dehydrated using ethanol with different concentrations (95%, 100%, 100%) for 10 min each. The dehydrated cells were dried using hexamethyl disilylamine and characterized by SEM.

Influence of pH on the Capture of Cells: CCRF-CEM was centrifuged and re-dispersed at a final concentration of 3×10^6 cells mL^{-1} in PBS solution with different pH values (7.4, 7.7, 8.0, 8.5, 9.0). A 20 μL of CCRF-CEM solution was dropped onto the EP-20APBA-200NaF-20 mV substrate and incubated at 37 °C for 60 min. Then, the substrate was rinsed with PBS for three times, stained by AO for 10 min and observed using a fluorescence inversion microscope system.

Influence of the Incubating Time on the Capture of Cells: CCRF-CEM was centrifuged and re-dispersed at a final concentration of 3×10^6 cells mL^{-1} in PBS solution (pH 8.0). A 20 μL of CCRF-CEM solution was dropped onto the EP-20APBA-200NaF-20 mV substrate and incubated at 37 °C for different time (5, 10, 20, 30, 45, 60 min). The captured cells were rinsed, stained by AO and observed by a fluorescence inversion microscope.

Release of Captured Cells from Poly-APBA Nanostructured Interfaces: 20 μL of CCRF-CEM (3×10^6 cells mL^{-1}) was incubated on the EP-20APBA-200NaF-20 mV substrate at 37 °C for 60 min. Then, it was rinsed, stained by AO. After that, 100×10^{-3} M fructose prepared in PBS solution (pH 8.0) was added to the nanostructured substrate with gently

© 2015 WILEY-VCH Verlag GmbH & Co. KGaA, Weinheim

shaking to release the captured cells through the strong interactions between boric acid and fructose. Fluorescence inversion microscope system was used to observe CCRF-CEM captured on EP-20APBA-200NaF-20 mV before and after release.

Cell Viability Analysis: AO and PI were used to stain and study the viability of captured cells before and after release. CCRF-CEM captured on the EP-20APBA-200NaF-20 mV substrate was stained using AO/PI kit according to the manufacturer's instructions. Then, the cells were rinsed with PBS and observed under a fluorescence inversion microscope. Cell viability analysis was taken by distinguishing the different colors of the stained cells. CCRF-CEM released from the substrates were collected, stained by AO/PI and dropped on the hemocytometer. The cell viability after release was analyzed by fluorescence imaging.

Supporting Information

Supporting Information is available from the Wiley Online Library or from the author.

Acknowledgements

This work was supported by the grants from the National 973 Basic Research Program (2012CB933800) and the National Natural Science Foundation of China (21275070, 21275071, 21327902).

Received: June 13, 2015
Revised: August 18, 2015
Published online: September 14, 2015

[1] H. J. Yoon, M. Kozminsky, S. Nagrath, *ACS Nano* **2014**, *8*, 1995.
[2] A. F. Chambers, A. C. Groom, I. C. MacDonald, *Nat. Rev. Cancer* **2002**, *2*, 563.
[3] S. Y. Zheng, H. K. Lin, B. Lu, A. Williams, R. Datar, R. J. Cote, Y. C. Tai, *Biomed. Microdevices* **2011**, *13*, 203.
[4] R. Gertler, R. Rosenberg, K. Fuehrer, M. Dahm, H. Nekarda, J. R. Siewert, *Molecular Staging of Cancer*, Springer-Verlag, Berlin **2003**.
[5] Y. J. Hu, L. L. Fan, J. E. Zheng, R. Cui, W. Liu, Y. L. He, X. Li, S. Huang, *Cytom. Part A* **2010**, *77A*, 213.
[6] P. R. C. Gascoyne, S. Shim, *Cancers* **2014**, *6*, 545.
[7] B. Naume, E. Borgen, K. Beiske, T. K. Herstad, G. Ravnas, A. Renolen, S. Trachsel, K. ThraneSteen, S. Funderud, G. Kvalheim, *J. Hematother.* **1997**, *6*, 103.
[8] X. L. Liu, S. T. Wang, *Chem. Soc. Rev.* **2014**, *43*, 2385.
[9] P. C. Zhang, L. Chen, T. L. Xu, H. L. Liu, X. L. Liu, J. X. Meng, G. Yang, L. Jiang, S. T. Wang, *Adv. Mater.* **2013**, *25*, 3566.
[10] S. T. Wang, H. Wang, J. Jiao, K. J. Chen, G. E. Owens, K. I. Kamei, J. Sun, D. J. Sherman, C. P. Behrenbruch, H. Wu, H. R. Tseng, *Angew. Chem. Int. Ed.* **2009**, *48*, 8970.
[11] S. K. Lee, G. S. Kim, Y. Wu, D. J. Kim, Y. Lu, M. Kwak, L. Han, J. H. Hyung, J. K. Seol, C. Sander, A. Gonzalez, J. Li, R. Fan, *Nano Lett.* **2012**, *12*, 2697.
[12] X. L. Liu, L. Chen, H. L. Liu, G. Yang, P. C. Zhang, D. Han, S. T. Wang, L. Jiang, *NPG Asia Mater.* **2013**, *5*, e63.
[13] N. A. Zhang, Y. L. Deng, Q. D. Tai, B. R. Cheng, L. B. Zhao, Q. L. Shen, R. X. He, L. Y. Hong, W. Liu, S. S. Guo, K. Liu, H. R. Tseng, B. Xiong, X. Z. Zhao, *Adv. Mater.* **2012**, *24*, 2756.
[14] Y. Wan, M. A. I. Mahmood, N. Li, P. B. Allen, Y. T. Kim, R. Bachoo, A. D. Ellington, S. M. Iqbal, *Cancer* **2012**, *118*, 1145.
[15] J. X. Meng, H. L. Liu, X. L. Liu, G. Yang, P. C. Zhang, S. T. Wang, L. Jiang, *Small* **2014**, *10*, 3735.
[16] X. L. Liu, F. L. Zhang, Q. Wang, J. Gao, J. X. Meng, S. T. Wang, Z. Z. Yang, L. Jiang, *Small* **2014**, *10*, 4677.
[17] W. Q. Chen, S. N. Weng, F. Zhang, S. Allen, X. Li, L. W. Bao, R. H. W. Lam, J. A. Macoska, S. D. Merajver, J. P. Fu, *ACS Nano* **2013**, *7*, 566.
[18] H. J. Yoon, T. H. Kim, Z. Zhang, E. Azizi, T. M. Pham, C. Paoletti, J. Lin, N. Ramnath, M. S. Wicha, D. F. Hayes, D. M. Simeone, S. Nagrath, *Nat. Nanotechnol.* **2013**, *8*, 735.
[19] J. Sekine, S. C. Luo, S. Wang, B. Zhu, H. R. Tseng, H. Yu, *Adv. Mater.* **2011**, *23*, 4788.
[20] Z. Y. Zhang, N. C. Chen, S. H. Li, M. R. Battig, Y. Wang, *J. Am. Chem. Soc.* **2012**, *134*, 15716.
[21] T. T. Lee, J. R. Garcia, J. I. Paez, A. Singh, E. A. Phelps, S. Weis, Z. Shafiq, A. Shekaran, A. del Campo, A. J. Garcia, *Nat. Mater.* **2015**, *14*, 352.
[22] Q. Yu, J. Cho, P. Shivapooja, L. K. Ista, G. P. Lopez, *ACS Appl. Mater. Interfaces* **2013**, *5*, 9295.
[23] S. Hou, H. C. Zhao, L. B. Zhao, Q. L. Shen, K. S. Wei, D. Y. Suh, A. Nakao, M. A. Garcia, M. Song, T. Lee, B. Xiong, S. C. Luo, H. R. Tseng, H. H. Yu, *Adv. Mater.* **2013**, *25*, 1547.
[24] C. C. A. Ng, A. Magenau, S. H. Ngalim, S. Ciampi, M. Chockalingham, J. B. Harper, K. Gaus, J. J. Gooding, *Angew. Chem. Int. Ed.* **2012**, *51*, 7706.
[25] X. L. Yu, R. X. He, S. S. Li, B. Cai, L. B. Zhao, L. Liao, W. Liu, Q. Zeng, H. Wang, S. S. Guo, X. Z. Zhao, *Small* **2013**, *9*, 3895.
[26] W. Li, J. S. Wang, J. S. Ren, X. G. Qu, *Angew. Chem. Int. Ed.* **2013**, *52*, 6726.
[27] W. Li, J. S. Wang, J. S. Ren, X. G. Qu, *Adv. Mater.* **2013**, *25*, 6737.
[28] S. Hou, L. B. Zhao, Q. L. Shen, J. H. Yu, C. Ng, X. J. Kong, D. X. Wu, M. Song, X. H. Shi, X. C. Xu, W. H. Ouyang, R. X. He, X. Z. Zhao, T. Lee, F. C. Brunicardi, M. A. Garcia, A. Ribas, R. S. Lo, H. R. Tseng, *Angew. Chem. Int. Ed.* **2013**, *52*, 3379.
[29] G. Springsteen, B. H. Wang, *Tetrahedron* **2002**, *58*, 5291.
[30] Z. B. Qu, X. G. Zhou, L. Gu, R. M. Lan, D. D. Sun, D. J. Yu, G. Y. Shi, *Chem. Commun.* **2013**, *49*, 9830.
[31] L. Zhang, Z. Y. Zhang, R. P. Liang, Y. H. Li, J. D. Qiu, *Anal. Chem.* **2014**, *86*, 4423.
[32] Y. H. Li, L. Zhang, J. Huang, R. P. Liang, J. D. Qiu, *Chem. Commun.* **2013**, *49*, 5180.
[33] W. Wu, H. R. Zhu, L. Z. Fan, D. F. Liu, R. Renneberg, S. H. Yang, *Chem. Commun.* **2007**, *23*, 2345.
[34] K. Djanashvili, L. Frullano, J. A. Peters, *Chem. Eur. J.* **2005**, *11*, 4010.
[35] S. Q. Liu, L. Bakovic, A. C. Chen, *J. Electroanal. Chem.* **2006**, *591*, 210.
[36] S. Q. Liu, B. Miller, A. C. Chen, *Electrochem. Commun.* **2005**, *7*, 1232.
[37] A. E. Ivanov, H. A. Panahi, M. V. Kuzimenkova, L. Nilsson, B. Bergenstahl, H. S. Waqif, M. Jahanshahi, I. Y. Galaev, B. Mattiasson, *Chem. Eur. J.* **2006**, *12*, 7204–7214.
[38] X. Zhong, H. J. Bai, J. J. Xu, H. Y. Chen, Y. H. Zhu, *Adv. Funct. Mater.* **2010**, *20*, 992.
[39] F. Kuralay, S. Sattayasamitsathit, W. Gao, A. Uygun, A. Katzenberg, J. Wang, *J. Am. Chem. Soc.* **2012**, *134*, 15217.
[40] H. L. Liu, Y. Y. Li, K. Sun, J. B. Fan, P. C. Zhang, J. X. Meng, S. T. Wang, L. Jiang, *J. Am. Chem. Soc.* **2013**, *135*, 7603.
[41] G. Q. Pan, B. B. Guo, Y. Ma, W. G. Cui, F. He, B. Li, H. L. Yang, K. J. Shea, *J. Am. Chem. Soc.* **2014**, *136*, 6203.
[42] S. Bhadra, D. Khastgir, N. K. Singha, J. H. Lee, *Prog. Polym. Sci.* **2009**, *34*, 783.
[43] D. H. Zhang, Y. Y. Wang, *Mater. Sci. Eng. B* **2006**, *134*, 9.
[44] J. X. Huang, R. B. Kaner, *Chem. Commun.* **2006**, *4*, 367.
[45] J. Stejskal, I. Sapurina, M. Trchova, *Prog. Polym. Sci.* **2010**, *35*, 1420.
[46] B. A. Deore, I. Yu, J. Woodmass, M. S. Freund, *Macromol. Chem. Phys.* **2008**, *209*, 1094.
[47] B. A. Deore, M. S. Freund, *Macromolecules* **2009**, *42*, 164.

© 2015 WILEY-VCH Verlag GmbH & Co. KGaA, Weinheim

[48] G. C. Li, Y. M. Li, H. R. Peng, K. Z. Chen, *Macromol. Rapid Commun.* **2011**, *32*, 1195.
[49] L. H. C. Mattoso, S. K. Manohar, A. G. Macdiarmid, A. J. Epstein, *J. Polym. Sci. Pol. Chem.* **1995**, *33*, 1227.
[50] M. Nicolas, B. Fabre, G. Marchand, J. Simonet, *Eur. J. Org. Chem.* **2000**, *9*, 1703.
[51] H. D. Tran, R. B. Kaner, *Chem. Commun.* **2006**, *37*, 3915.
[52] J. Yano, K. Sanada, R. Patil, Y. Ooyama, K. Komaguchi, Y. Harima, *Mater. Chem. Phys.* **2007**, *106*, 279.
[53] L. Dennany, P. C. Innis, F. Masdarolomoor, G. G. Wallace, *J. Phys. Chem. B* **2010**, *114*, 2337.
[54] M. C. Bernard, A. Hugot-Le Goff, *Electrochim. Acta* **2006**, *52*, 595.
[55] A. E. Ivanov, I. Y. Galaev, B. Mattiasson, *J. Mol. Recognit.* **2006**, *19*, 322.
[56] C. J. Bettinger, R. Langer, J. T. Borenstein, *Angew. Chem. Int. Ed.* **2009**, *48*, 5406.
[57] M. J. Dalby, N. Gadegaard, M. O. Riehle, C. D. W. Wilkinson, A. S. G. Curtis, *Int. J. Biochem. Cell Biol.* **2004**, *36*, 2005.
[58] J. Albuschies, V. Vogel, *Sci. Rep.* **2013**, *3*, 1658.
[59] K. M. Molapo, P. M. Ndangili, R. F. Ajayi, G. Mbambisa, S. M. Mailu, N. Njomo, M. Masikini, P. Baker, E. I. Iwuoha, *Int. J. Electrochem. Sci.* **2012**, *7*, 11859.
[60] D. E. Stilwell, S. M. Park, *J. Electrochem. Soc.* **1988**, *135*, 2254.

© 2015 WILEY-VCH Verlag GmbH & Co. KGaA, Weinheim